

Signatures of electron-boson coupling in half-metallic ferromagnet Mn_5Ge_3 : study of electron self-energy $\Sigma(\omega)$ obtained from infrared spectroscopy

S. V. Dordevic,^{1,*} N. Stojilovic,² L. W. Kohlman,¹ Rongwei Hu,^{3,4} and C. Petrovic³

¹*Department of Physics, The University of Akron, Akron, Ohio 44325 USA*

²*Physics Department, John Carroll University, University Heights, OH 44118 USA*

³*Condensed Matter Physics and Materials Science Department,
Brookhaven National Laboratory, Upton, New York 11973, USA*

⁴*Department of Physics, Brown University, Providence, RI 02912, USA*

(Dated: November 16, 2018)

We report results of our infrared and optical spectroscopy study of a half-metallic ferromagnet Mn_5Ge_3 . This compound is currently being investigated as a potential injector of spin polarized currents into germanium. Infrared measurements have been performed over a broad frequency (50 - 50000 cm^{-1}) and temperature (10 - 300 K) range. From the complex optical conductivity $\sigma(\omega)$ we extract the electron self-energy $\Sigma(\omega)$. The calculation of $\Sigma(\omega)$ is based on novel numerical algorithms for solution of systems of non-linear equations. The obtained self-energy provides a new insight into electron correlations in Mn_5Ge_3 . In particular, it reveals that charge carriers may be coupled to bosonic modes, possibly of magnetic origin.

PACS numbers: 78.20.Ci, 78.30.-j, 74.25.Gz

Half-metallic ferromagnetism (HMFM) was first discovered in half-Heusler alloy NiMnSb [1]. Band structure calculations showed that all electrons at the Fermi level had the same spin orientation, resulting in a spin-polarized ferromagnetic state [2, 3, 4]. This was in stark contrast with conventional metals like gold or copper, in which there is an equal population of spin-up and spin-down electrons, resulting in a non-magnetic ground state. The inset of Fig. 1 displays schematic one-electron band structure of HMFM. In an ideal case, the number of electrons at the Fermi level with one spin orientation is zero (minority spin electrons), i.e. all electrons have the opposite spin orientation (majority spin electrons). In real materials there may be electrons with both spin polarizations at the Fermi level. Their number is characterized through the so-called spin polarization $P = (N_{\uparrow} - N_{\downarrow}) / (N_{\uparrow} + N_{\downarrow})$ [5].

In this work we have used infrared (IR) spectroscopy to study Mn_5Ge_3 , an intermetallic compound shown to exhibit HMFM with a Curie temperature of $T_C \simeq 293$ K [6]. Mn_5Ge_3 crystallizes in a hexagonal crystal structure, space group $P63/mcm$, with lattice parameters $a = 7.191$ Å and $c = 5.054$ Å. The anisotropic crystal structure results in slightly anisotropic transport and thermodynamic properties [7, 8]. Recent theoretical calculations and spin-sensitive point contact Andreev reflection measurements have shown that Mn_5Ge_3 has a substantial spin polarization in the range 43-54 % [9]. In addition to its unusual properties from the fundamental point of view, Mn_5Ge_3 has also attracted attention as a potential injector of spin-polarized currents into germanium (Ge) [9, 10]. Thin films of Mn_5Ge_3 have been successfully grown on Ge(111) using solid phase epitaxy [10]. This important technological advance opens the door for integration of Mn_5Ge_3 with the existing Ge technologies and

possible spintronics applications.

Reflection measurements on single crystal Mn_5Ge_3 have been performed over a broad frequency range from about 50 cm^{-1} to 50000 cm^{-1} (6 meV – 6.2 eV) and at temperatures from 10 K up to room temperature. An overfilling technique was used to obtain the absolute values of reflectance from a sample with surface area of approximately 1 mm \times 1 mm [11]. From the measured reflectance $R(\omega)$, complex optical conductivity $\sigma(\omega) = \sigma_1(\omega) + i\sigma_2(\omega)$ was obtained through Kramer-Kronig (KK) transformation [12, 13].

Figure 1 displays raw reflectance data $R(\omega)$ and the real part of optical conductivity $\sigma_1(\omega)$. The overall behavior of both optical functions is metallic, however there are some features that distinguish it from conventional metals [14]. One can identify three contributions to $\sigma_1(\omega)$: i) a Drude-like peak at zero frequency which narrows as temperature decreases, ii) a region of relatively constant conductivity (between about 1000 and 10000 cm^{-1}) and iii) a region of interband transitions above 10000 cm^{-1} . We also note that similar three contributions to $\sigma_1(\omega)$ were observed in some other HMFL, such as CrO_2 [15] and in NiMnSb [16].

To gain further insight into electronic properties of Mn_5Ge_3 we employed a standard Drude-Lorentz (DL) model [12, 13, 14]. The minimal model to achieve a good fit consisted of a Drude and two Lorentzian modes, centered at around 1480 cm^{-1} and 18000 cm^{-1} . The total fit, as well as the three individual contributions, are shown in Fig. 1(b) with gray lines. The oscillator at 18000 cm^{-1} simulates the effect of interband transitions. On the other hand, the oscillator at 1480 cm^{-1} seems to indicate the presence of low-lying transition and we tentatively assign it to excitations across the spin-flip gap (Δ_{sf} in Fig. 1). We will come back to this important

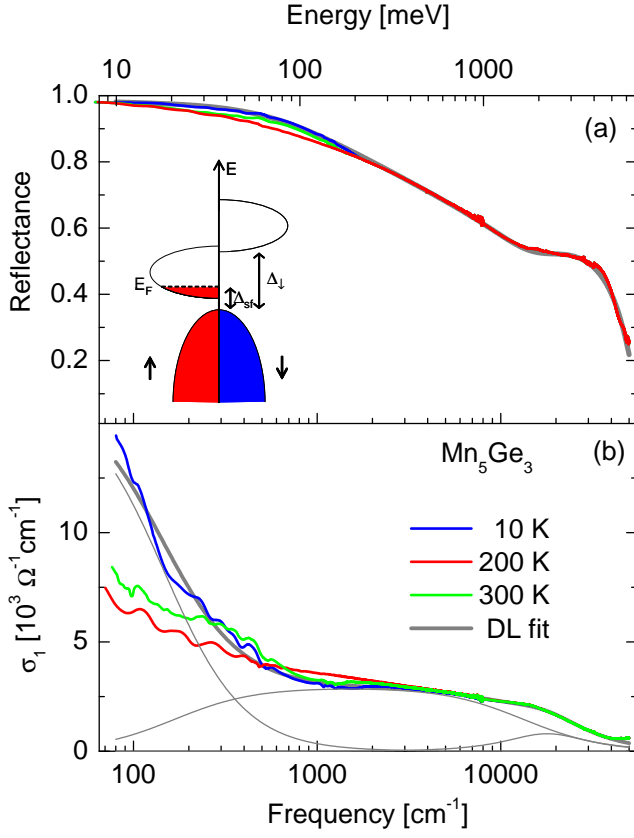


FIG. 1: (Color online). (a) Reflectance of Mn_5Ge_3 at several selected temperatures between 10 and 290 K. The temperature dependence is limited mostly to the region below about 1500 cm^{-1} . The inset represents a schematic band structure for a half-metallic ferromagnet, the bands for spin-up and spin-down electrons plotted separately [2, 3, 4]. The energy gap for minority spin electrons is Δ_{\downarrow} , and the spin-flip gap is Δ_{sf} . (b) The optical conductivity $\sigma_1(\omega)$ obtained from reflectance using KK transformation. Also shown with gray lines are the total DL fit at 10 K, as well as the three individual components of the fit.

point below.

In the one-component approach, one assumes that only a single type of carriers are present in the system, but their scattering rate acquires frequency dependence [12, 13, 14]. Within the so-called "extended" Drude model one calculates the *optical* scattering rate $1/\tau(\omega)^{op}$ and effective mass $m^*(\omega)^{op}/m_b$ from the optical conductivity $\sigma(\omega)$ as:

$$\frac{1}{\tau(\omega)^{op}} = \frac{\omega_p^2}{4\pi} \Re \left[\frac{1}{\sigma(\omega)} \right] \quad (1)$$

$$\frac{m^*(\omega)^{op}}{m_b} = \frac{\omega_p^2}{4\pi} \Im \left[\frac{1}{\sigma(\omega)} \right] \frac{1}{\omega} \quad (2)$$

where the plasma frequency $\omega_p^2 = 4\pi e^2 n/m_b$ (n is the carrier density and m_b their band mass) is estimated from the integration of $\sigma_1(\omega)$ up to the frequency of the onset

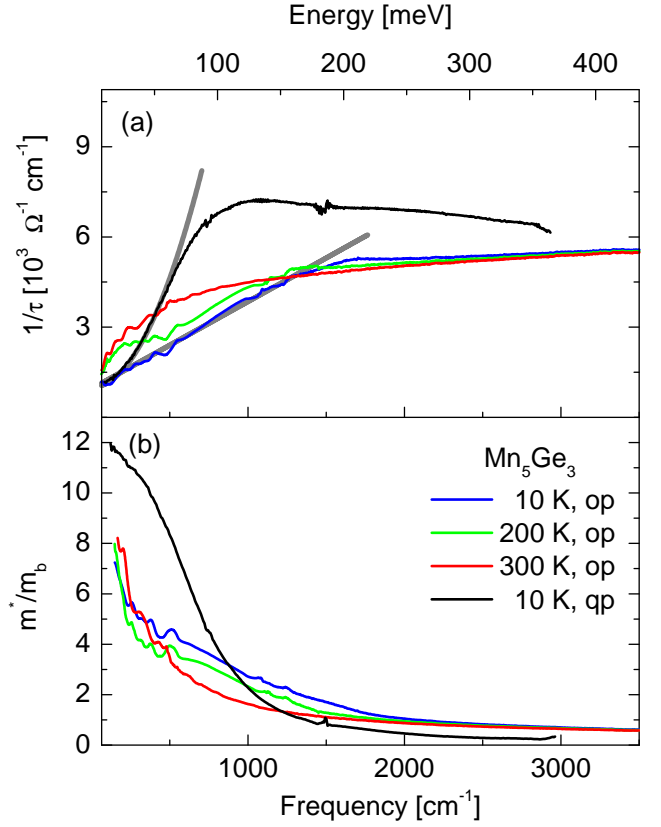


FIG. 2: (Color online). Optical scattering rate $1/\tau(\omega)^{op}$ and effective mass $m^*(\omega)^{op}/m_b$ obtained from Eqs. 1 and 2. Also shown are the quasiparticle scattering rate $1/\tau(\omega)^{qp}$ and effective mass $m^*(\omega)^{qp}/m_b$ at 10 K, as defined in the text.

of interband absorption (the cut-off frequency). By integrating the optical conductivity up to 10000 cm^{-1} we get $\omega_p = 33000 \text{ cm}^{-1}$ (4.1 eV) [17]. However the value of plasma frequency obtained this way is ambiguous, as it depends on the choice of the cut-off frequency, i.e. the separation of intra- and inter-band contributions. The results of extended Drude analysis are shown in Fig. 2. The optical scattering rate $1/\tau(\omega)^{op}$ displays almost linear frequency dependence, and characteristic suppression below about 1500 cm^{-1} . This is very close to the frequency of the low-lying transitions obtained from DL fits. We also point out that similar suppression of scattering rate was observed in the spectra of HMFMs CrO_2 [15] and NiMnSb [16].

To elucidate this behavior we employ an alternative approach of quantifying correlation effects: we calculate the electron self-energy $\Sigma(\omega)$ directly from $\sigma(\omega)$. Similar procedure was used before in studies of superconductors [18, 19]. Electron self-energy is a physical quantity of significant interest, as it contains important information about electron interactions in a solid. In general, it is a complex function of frequency, $\Sigma(\omega) = \Sigma_1(\omega) + i\Sigma_2(\omega)$, where its real part, $\Sigma_1(\omega)$, is related to quasiparticle energy renormalization and the imaginary part $\Sigma_2(\omega)$ corresponds to quasiparticle life-time.

Hwang et al. introduced [20, 21] *optical* self-energy $\Sigma^{op}(\omega)$, which has been used frequently in the analysis of IR data [23, 24, 25]. $\Sigma^{op}(\omega)$ is defined as:

$$\sigma(\omega) = \frac{i\omega_p^2}{\omega - 2\Sigma^{op}(\omega)} \quad (3)$$

and it can be calculated from $\sigma(\omega)$ using an analytic transformation. It is easy to show that $1/\tau(\omega)^{op} = -2\Sigma_2^{op}(\omega)$ and $\omega(m^*(\omega)^{op}/m_b - 1) = -2\Sigma_1^{op}(\omega)$. Here we calculate the electron self-energy directly from its relation to $\sigma(\omega)$ at T= 0 K [26, 27, 28]:

$$\sigma(\omega) = \frac{i\omega_p^2}{4\pi\omega} \int_0^\omega \frac{d\omega'}{\omega - \Sigma(\omega' + \omega) + \Sigma^*(\omega')}. \quad (4)$$

This expression reduces to Eq. 3 as the first order approximation in ω [27]. When discretized, Eq. 4 becomes:

$$\sigma_k = \frac{i\omega_p^2}{4\pi\omega_k} \sum_{j=1}^k \frac{\Delta\omega}{\omega_k - \Sigma_{j+k} + \Sigma_j^*}, \quad (5)$$

where $\sigma_k = \sigma(\omega_k)$, $\Sigma_k = \Sigma(\omega_k)$, $k=1, \dots, N$, and N is the number of (equidistant) points at which we perform the inversion. Eq. 5 effectively represents a system of $2N$ *non-linear* equations with $2N$ unknowns (Σ_{1k} and Σ_{2k}), but since $\Sigma(\omega)$ is a response function, its real and imaginary parts are related through a KK transformation. Thus the problem reduces to a system of N equations with N unknowns (for example Σ_{2k}). However it is an inverse problem and is also ill-posed.

Ill-posed inverse problems can be solved using, for example, the Levenberg-Marquardt algorithm [29]. To suppress numerical instabilities, the problem must first be regularized [29]. We have employed first order Tikhonov regularization, which seems to give the best results. The solution of the system starts from an initial guess and proceeds iteratively, until it has converged to within the required accuracy. An interesting choice for the starting point of iteration is $\Sigma^{op}(\omega)$ from Eq. 3. One also must ensure that the system converges to the same solution from several different starting points.

Figure 3 displays the results of inversion calculations for Mn_5Ge_3 at 10 K, as well as the optical self-energy $\Sigma^{op}(\omega)$ from Eq. 3. As can be seen, there are some differences between $\Sigma(\omega)$ and $\Sigma^{op}(\omega)$. By analogy with the optical scattering rate $1/\tau(\omega)^{op}$ (Eq. 1) and effective mass $m^*(\omega)^{op}/m_b$ (Eq. 2) we introduce *quasiparticle* scattering rate as $1/\tau(\omega)^{qp} = -2\Sigma_2(\omega)$ and *quasiparticle* effective mass as $\omega(m^*(\omega)^{qp}/m_b - 1) = -2\Sigma_1(\omega)$. These two new quantities are shown in Fig. 2, and they also differ from their optical counterparts. Most notably, the lower energy suppression of scattering rate follows a power-law behavior: $1/\tau(\omega)^{qp} \simeq \omega^2$, whereas $1/\tau(\omega)^{op} \simeq \omega$ (gray

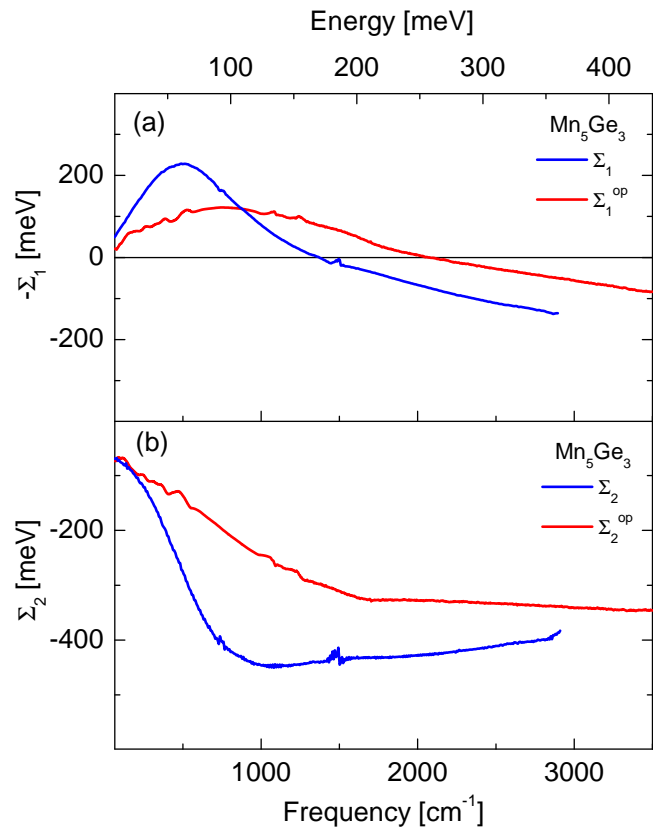


FIG. 3: (Color online). Real and imaginary parts of self-energy $\Sigma(\omega)$ obtained from the numerical inversion of Eq. 5. Also shown are the real and imaginary parts of optical self-energy $\Sigma^{op}(\omega)$ calculated from Eq. 3.

lines in Fig. 2). These important differences warrant further theoretical considerations.

As mentioned above, the low frequency suppression of scattering rate observed in Mn_5Ge_3 was also found in CrO_2 and NiMnSb , and appears to be generic to all HMFMs. The suppression $1/\tau(\omega)$ can be explained as a consequence of HMFMs band structure (inset of Fig. 1). Namely, in the one-electron picture, the low-energy minority spin excitations (spin-flip processes) are forbidden because of the lack of available states [2]. This scenario seems to work well in CrO_2 where the scattering rate drops to very low values below about 500 cm^{-1} , which was assigned to spin-flip gap [15]. In Mn_5Ge_3 the scattering rate does not drop to zero, but is, instead, suppressed following a power-law dependence. This behavior can, in principle, be explained as due to peculiarities of the density of states [30]. We propose an alternative explanation in terms of the low-energy scattering channels. They require one to go beyond the one-electron picture [2]. Namely, when electron correlations are taken into account, the low-energy spin-flip excitations become possible because of a coupling of majority spin electrons and virtual magnons [2]. This coupling is believed to be of prime importance for transport processes in HMFMs (and ferromagnets in general).

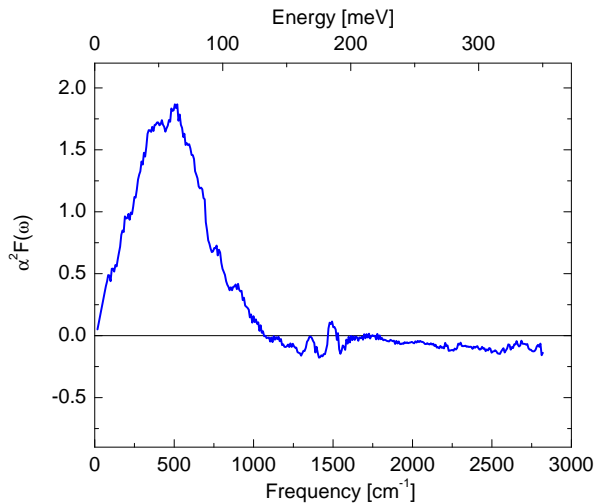


FIG. 4: (Color online). The electron-boson spectral function $\alpha^2 F(\omega)$ of Mn_5Ge_3 calculated from $\Sigma_2(\omega)$.

Coupling of charge and bosonic degrees of freedom has been known to be important in solids. In optical functions this coupling shows up as a suppression of scattering rate [12, 13, 31]. A quantity that contains all of the information about such coupling is the electron-boson spectral function $\alpha^2 F(\omega)$, which can be obtained from $\Sigma(\omega)$ as $-\pi\alpha^2 F(\omega) = d\Sigma_2(\omega)/d\omega$ [28]. $\alpha^2 F(\omega)$ calculated this way is shown in Fig. 4 and, as could be anticipated from $1/\tau(\omega)^{qp}$, it is characterized by a pronounced peak centered at about 500 cm^{-1} (60 meV). This peak indicates that charge carriers may be coupled to bosonic modes, such as magnons. Note however that in Mn_5Ge_3 the spin-polarization is only partial [9], which implies that other scattering channels (such as phonons) are also possible. Further experimental tests, such as magneto-optical measurements, will help elucidate if this scenario applies to Mn_5Ge_3 , as well as the contributions of various scattering channels.

High Curie temperature, substantial degree of spin polarization, and a good lattice match with germanium and silicon make Mn_5Ge_3 a very promising candidate for an injector of spin-polarized currents. Recently discovered [32] simultaneous enhancement of both spin polarization and Curie temperature in Fe-doped Mn_5Ge_3 above room temperature opens new and exciting possibilities for controlled spin injection in functional spintronics devices. In this work we used IR spectroscopy to study electronic properties of Mn_5Ge_3 . Our results reveal the spin-flip gap of approximately 1500 cm^{-1} (186 meV). The inversion procedure described allows access to electron self-energy from IR, and more direct (and quantitative) comparisons with photoemission spectroscopy. Both optical and quasiparticle scattering rates reveal a power-law behavior (albeit with different exponents), which might signal coupling of charge carriers to bosonic modes, possibly of magnetic origin.

We thank K.S. Burch for bringing Ref. [18] to our at-

tention and D.N. Basov, C.C. Homes, V.Yu. Irkhin and T. Timusk for critical reading of the manuscript. Special thanks to R.D. Ramsier for the use of his equipment. Part of this research was carried out at the Brookhaven National Laboratory, which is operated for the U.S. Department of Energy by Brookhaven Science Associates (DE-AC02-98CH10886).

* Electronic address: dsasa@uakron.edu

- [1] R.A. de Groot, F.M. Mueller, P.G. van Engen and K.H.J. Buschow, *Physical Review Letters* **50**, 2024 (1983).
- [2] M.I. Katsnelson, V.Yu. Irkhin, L. Chioncel, A.I. Lichtenstein and R.A. de Groot, *Reviews of Modern Physics* **80**, 315 (2008).
- [3] V.Yu. Irkhin and M.I. Katsnelson, *Physics Uspekhi* **37**, 659 (1994).
- [4] W.E. Pickett and J.S. Moodera, *Physics Today* **54**, 39 (2001).
- [5] I.I. Mazin, *Physical Review Letters* **83**, 1427 (1999).
- [6] R. Fontaine and R. Pauthenet, *Comptes rendus* **254**, 650 (1962).
- [7] C. Petrovic et al., unpublished.
- [8] S. Picozzi, A. Continenza and A.J. Freeman, *Physical Review B* **70**, 235205 (2004).
- [9] R.P. Panguluri, Changgan Zeng, H.H. Weitering, J.M. Sullivan, S.C. Erwin and B. Nadgorny, *Physica Status Solidi (b)* **242**, R67 (2005).
- [10] C. Zeng, S.C. Erwin, L.C. Feldman, A.P. Li, R. Jin, Y. Song, J.R. Thompson and H.H. Weitering, *Applied Physics Letters* **83**, 5002 (2003).
- [11] C.C. Homes, M.A. Reedyk, D.A. Crandles and T. Timusk, *Applied Optics* **32**, 2976 (1993).
- [12] D.N. Basov and T. Timusk, *Reviews of Modern Physics* **77**, 721 (2005).
- [13] S.V. Dordevic and D.N. Basov, *Annalen der Physik* **15**, 545 (2006).
- [14] M. Dressel and G. Gruner, *Electrodynamics of Solids*, Cambridge University Press, Cambridge (2001).
- [15] E.J. Singley, C.P. Weber, D.N. Basov, A. Barry and J.M.D. Coey, *Physical Review B* **60**, 4126 (1999).
- [16] F.B. Mancoff, B.M. Clemens, E.J. Singley and D.N. Basov, *Physical Review B* **60**, R12565 (1999).
- [17] This value cannot be directly compared with these obtained from numerical calculations [8] because IR cannot resolve the two spin directions.
- [18] Tae-Hyoung Gimm and Han-Yong Choi, cond-mat/0212361.
- [19] Tae-Hyoung Gimm and Han-Yong Choi, *International Journal of Modern Physics B* **17**, 3534 (2003).
- [20] J. Hwang, T. Timusk and G. D. Gu, *Nature* **427**, 714 (2004).
- [21] Hwang et al. [22] have also introduced a quantity $\Sigma^{op-qp} \equiv d[\omega\Sigma^{op}(\omega)]/d\omega$.
- [22] J. Hwang, E.J. Nicol, T. Timusk, A. Knigavko and J.P. Carbotte, *Physical Review Letters* **98**, 207002 (2007).
- [23] E. van Heumen, E. Muhlethaler, A.B. Kuzmenko, D. van der Marel, H. Eisaki, M. Greven, W. Meevasana and Z.X. Shen, arXiv:0807.1730.
- [24] M.M. Qazilbash, J.J. Hamlin, R.E. Baumbach, M.B.

- Maple and D.N. Basov, arXiv:0808.3748
- [25] J. Hwang, J.P. Carbotte and T. Timusk, Physical Review Letters **100**, 177005 (2008).
- [26] P.B. Allen, Physical Review B **3**, 305 (1971).
- [27] P.B. Allen, cond-mat/0407777.
- [28] M.R. Norman and A.V. Chubukov, Physical Review B **73**, 140501(R) (2006).
- [29] W.H. Press, S.A. Teukolsky and W.T. Vetterling and B.P. Flannery, *Numerical Recipes*, Cambridge University Press (2002), and references therein.
- [30] S.G. Sharapov and J.P. Carbotte, Physical Review B **72**, 134506 (2005).
- [31] S.V. Dordevic, C.C. Homes, J.J. Tu, T. Valla, M. Strongin, P.D. Johnson, G.D. Gu and D.N. Basov, Physical Review B **71**, 104529 (2005).
- [32] T.Y. Chen, C.L. Chien and C. Petrovic, Applied Physics Letters **91**, 142505 (2007).